The International Journal of Advanced Manufacturing Technology (2020) 108:553–570
https://doi.org/10.1007/s00170-020-05391-x

ORIGINAL ARTICLE

Effect of print orientation and bronze existence on tribological and mechanical properties of 3D-printed bronze/PLA composite

Muammel M. Hanon[1,2] · Yazan Alshammas[3] · László Zsidai[3]

Received: 19 July 2019 / Accepted: 1 May 2020 / Published online: 16 May 2020

Abstract

In this work, fused deposition modeling (FDM) technology is employed for manufacturing tribological and tensile testing specimens. The test pieces are fabricated in diverse directions to examine the influence of print orientation. The tribological tests are carried out in reciprocating sliding and under dry condition. Due to their relevance, the surface roughness and the hardness of the products are studied as well. Many images are captured under a microscope to better understand the surface morphology of 3D-printed parts before and after testing. The findings reveal that the existence of various print orientations determines differences in mechanical properties and tribological behavior. Among the investigated parameters, the one with the highest tensile strength at break point is the On-Edge print orientation. The vertically oriented test pieces offer the highest friction tendency but the lowest wear depth. Meanwhile, less wear is observed when sliding under low loads but the tendency for stick-slip phenomenon occurrence increases. Although PLA is presently one of the most popular filaments for 3D printing, it can be employed in some industrial applications (e.g., bushings and bearings), if the tribological properties are amended. Bronze is characterized by excellent sliding capability because of its very low metal-on-metal friction. To date, very limited attention has been given to research on the tribology of 3D-printed objects. Therefore, the purpose of the current work is to fill the gap in knowledge by being the first study to evaluate the impact of bronze presence and 3D printing orientation on the tribological properties of bronze/PLA composite.

Keywords Additive manufacturing · Polymer composites · Coefficient of friction · Wear · 3D printing parameters

1 Introduction

Fused deposition modeling (FDM) is a revolutionary technology that enables higher printing speed and is more affordable in comparison with other 3D printing methods [1]. Therefore, its printers are currently the most common consumer-level 3D printers among those that are based on extrusion additive manufacturing (AM) for printing polymer composites [2]. The FDM technique uses a spool of thermoplastic material in the form of filaments (e.g., PLA, PETG, ABS, and PC) to be melted and then extruded utilizing a heated nozzle [3]. It has recently become possible to employ thermoplastics with higher melting temperatures (e.g., PEEK) as 3D printing materials [4].

In the last decade, considerable interest has been given to the use of thermoplastics in industrial applications, building, and various automobile components, such as door panels, dashboards, headliners, package trays, and interior parts [5]. Due to its good mechanical properties, sustainability, and biodegradability, polylactic acid (PLA) has been extensively employed in numerous implementations [6]. However, PLA has some limitations such as low impact strength, water sensitivity, and high brittleness [7]. This issue could be overcome by reinforcing the bulk of the material through the addition of fibers or fillers, which is a convenient way to engineer the physical, mechanical, and thermal properties and therefore to improve performance [8]. There is a steady increase in the number of studies on the 3D printing of reinforced

✉ Muammel M. Hanon
Sharba.Muammel.M.Hanon@phd.uni-szie.hu

[1] Mechanical Engineering Doctoral School, Szent István University, Gödöllő 2100, Hungary

[2] Baquba Technical Institute, Middle Technical University (MTU), Baghdad, Iraq

[3] Institute for Mechanical Engineering Technology, Faculty of Mechanical Engineering, Szent István University, Gödöllő 2100, Hungary

thermoplastic polymers. The effect of reinforcement with carbon fiber [9, 10], glass fiber [11], wood content [12], denim (a twilled cotton fabric) [13], and microcrystalline cellulose [14] has already been reviewed.

Among the print parameters, print orientation, raster direction angle, infill percentage and pattern, and layer thickness are the most critical settings that influence the properties of 3D-printed polymers using FDM technology [15]. The impact of these parameters on the mechanical properties, particularly tensile properties, has been studied extensively in the literature [16–25]. Polymeric products are suitable for tribological applications due to their unique properties, such as self-lubrication, vibration-damping ability, and corrosion resistance [26]. In spite of this, only a few studies have so far investigated the tribology of 3D-printed parts [27, 28]. Bustillos et al. [29] inspected the wear and friction of 3D-printed graphene-reinforced PLA composites by the FDM technique. The results revealed that the presence of graphene enhanced the wear resistance by 14%, while the friction coefficient behavior displayed a reduction of 65% as compared with the initial PLA. The authors argued that these promising findings proved that PLA-graphene was viable for use as orthopedic scaffold. The structural and tribological properties of 3D-printed biocarbon-reinforced PLA filaments were reviewed by Ertane et al. [30]. They disclosed that wear volume was decreased significantly in the sample manufactured with 30 vol.-% carbon. The occurrence of some signs was indicative of fatigue and abrasive wear mechanism. The case of reinforcement showed fewer fluctuations in the friction coefficient values, which remained at around 0.5. Bai et al. [31] studied the effect of surface orientation on the tribological properties of polyamide 12 (PA12) after selective laser sintering (SLS). The wear properties revealed anisotropic behavior. Tribological test findings showed that the friction coefficient was smaller and wear resistance was greater for the side surfaces in comparison with the top surfaces. The aforementioned studies prove that the effect of the 3D printing structure of thermoplastic composites on wear and friction properties warrants greater attention.

Based on the literature, bronze has a significant role in improving the tribological properties of polymer composites. Unlu et al. [32] reported that adhesive wear tracks decreased in bearings made of bronze-reinforced poly-tetra-fluoro-ethylene (PTFE) polymer composite owing to the good wear resistance property of bronze. The tribological properties of the reinforced PTFE bearings were improved two- or threefold. To investigate how PTFE properties could be improved, Conte and Igartua [33] performed a comparative analysis among seven PTFE composites, one of which was PTFE + 60 wt% bronze. They noticed the presence of hard and soft phases in the polymer matrix. The existence of those phases enhanced the self-lubricating of the matrix, which improved the tribological properties of PTFE. Unal et al. [34] stated that, under similar testing conditions, the bronze-reinforced PTFE composite exhibited high wear resistance and low coefficient of friction as compared with the pure PTFE polymer. The highest wear resistance was observed at 60% bronze-reinforced PTFE. The friction coefficient decreased under lighter load of up to 30 N, whereas it remained stable at a heavier load of more than 30 N. The applied load had a greater effect on the wear behavior than the sliding velocity. The PLA polymer is one of the most widely used materials for 3D printing nowadays, but in spite of this, its tribological properties have not been thoroughly investigated. Therefore, the current work utilizes PLA polymer reinforced with bronze (particle-filled) in a filament form to improve the tribological performance of 3D-printed parts.

The present work is concerned with the examination of the effect of fused deposition modeling process settings and the presence of bronze on the mechanical and tribological (in terms of wear and friction) behavior of 3D-printed bronze/PLA composite. In order to inspect the impact of the print orientation parameter, the specimens were printed in various orientations. For the tensile test, the orientations were Flat, On-Edge, and Upright, while for the tribological test, the orientations were Horizontal, 45° angle, and Vertical. The tribological properties were tested by employing reciprocating sliding tribometer under dry sliding conditions with a short stroke length and somewhat low speed. The behavior of the friction coefficient and wear depth versus the sliding distance was evaluated and compared for all the printed pieces. Printing accuracy and precision were studied and surface roughness and hardness were examined as well. The paper also discussed the surface structure of 3D-printed samples before and after tests.

2 Materials and methods

2.1 Print procedure and parameters

The commercially manufactured bronze/PLA filaments having a diameter of 1.75 mm were used to fabricate the 3D-printed tribology and tensile test specimens. The bronze/PLA filaments with a bronze content of 8% were purchased from a commercial 3D filament manufacturer [35]. The test pieces were produced using the commercial 3D printer WANHAO Duplicator 6 with a nozzle diameter of 0.4 mm in the additive manufacturing laboratory at Szent Istvan University, Hungary. The specimens were printed with a 45/135° raster angle. For slicing purposes, the Simplify 3D software was used. The printing temperature and platform temperature were maintained at 195 °C and 60 °C, respectively. Prior to testing, the specimens were conditioned in a climate room with a temperature of 25 °C and relative humidity of 50%.

The tensile test specimens were manufactured at three-print orientations, which were Flat (horizontally), On-Edge, and Upright (vertically) consecutively, as shown in Fig. 1a. In the case of On-Edge print orientation, the 3D-printed samples were fabricated with supporter beneath the gauge section due to the vast space. The tribology test samples were fabricated at three-print orientations as well, which were Horizontal, 45° angle, and Vertical respectively, as exhibited in Fig. 1b.

2.2 Print accuracy and precision

The accuracy in the 3D printing is how the dimensions of the measured product close to true (nominal) value. The true value represents the dimensions of the CAD model, whereas the consistent repeatability during measuring of measurement is known as precision. This is an essential point in additive manufacturing since it ultimately translates to reliability; count on the machine to fabricate the expected results for every print.

In this work, the accuracy and precision were inspected for the printed specimens. Concerning the tensile test sample, the much more important area is the gauge section. The dimensions of the gauge cross-section (width "*b*" and thickness "*h*") were measured at three spots (both ends and the middle), as shown in Fig. 1e and compared with the exact CAD design to determine the accuracy. Every identical test piece was repeated three times, and then the same measuring mechanism was applied to examine the precision. Regarding the cylindrical tribology test piece, both ends of the specimens were measured in *X* and *Y* directions to investigate the diameter. The length was measured three times at the marked points illustrated in Fig. 1d. For precision (repeatability) check, the standard deviation was calculated and evinced by error bars.

2.3 Tensile test

The 3D-printed test pieces were produced with dimensions of 150 mm by 20 mm by 4 mm according to the dog-bone tensile

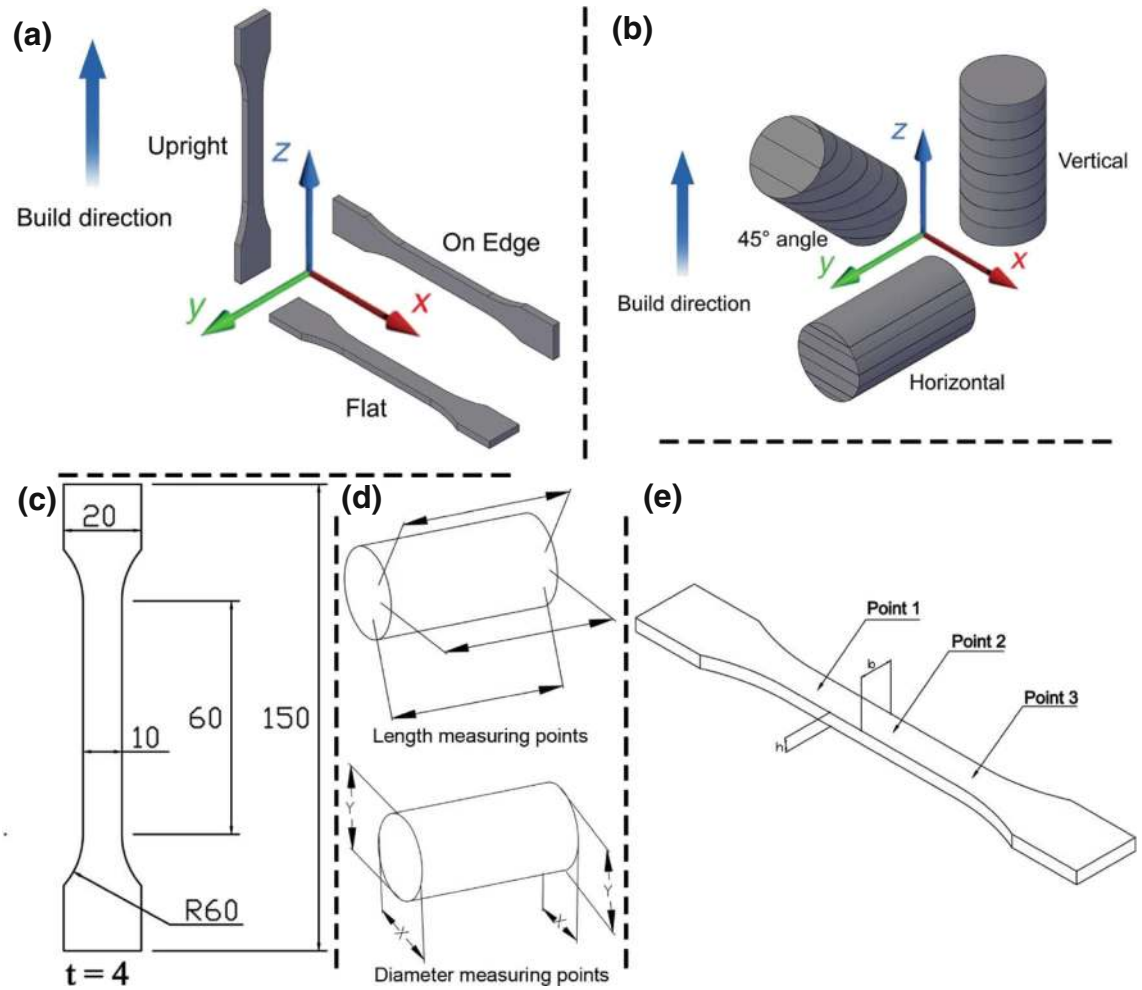

Fig. 1 **a** Print orientations of tensile test specimens; **b** print orientations of tribology test specimens; **c** dimensions of the used dog-bone tensile test piece; **d** length and diameter measurement points for the cylindrical tribology test samples; **e** the measurement points of gauge section dimensions (width "*b*" and thickness "*h*")

test geometry of the ISO 527-2: 2012 standard type 1B sample [36] as presented in Fig. 1c.

The tensile properties of the printed specimens (parallel to the printing orientation) were determined through tensile tests using a Zwick/Roell Z100 testing machine in accordance with ISO 527 [37]. Three specimens were tested for the tensile strength of each similar sample type. A test speed of 5 mm/min was performed. Prior to measurement, the samples were in a room with humidity of 45–50% for 24 h. Humidity has a significant impact on the measured values [38]; therefore, for match results, it was substantial that all the specimens had the same moisture content. The tensile test specimens before the experiment are exhibited in Fig. 2a.

2.4 Tribology test

A cylinder-on-plate reciprocating tribometer (PLINT TE 77 "High-Frequency friction machine" employed by Kalácska and Zsidai in previous research [39]) was used to evaluate the wear and friction characteristics of the utilized material. The schematic of the cylinder-on-plate apparatus is shown in Fig. 2b. The counterface is a ground steel plate (surface roughness 0.08 μm R_a) with a maximum stroke and frequency of 50 mm and 30 Hz respectively. Sliding occurs between a reciprocating cylinder clamped in the specimen holder and the stationary plate. Normal load, frequency, sliding speed, and stroke length can be varied to fit the test requirements.

The method for testing is a reciprocating linear sliding friction measurement without lubricants. Alternating motion is provided by a variable speed electric motor using the push rod attached to its axis. This motor provided with an adjustable frequency drive and an eccentric disc. The eccentric disc drives the sliding plate on a linear path by the coupled interchangeable push rod. The inverter is used to set the experiment frequency to the required value precisely. The stroke length could be modified according to the measurement parameters due to the eccentricity of the thrust bar. The static load of the test is determined before starting the measurement.

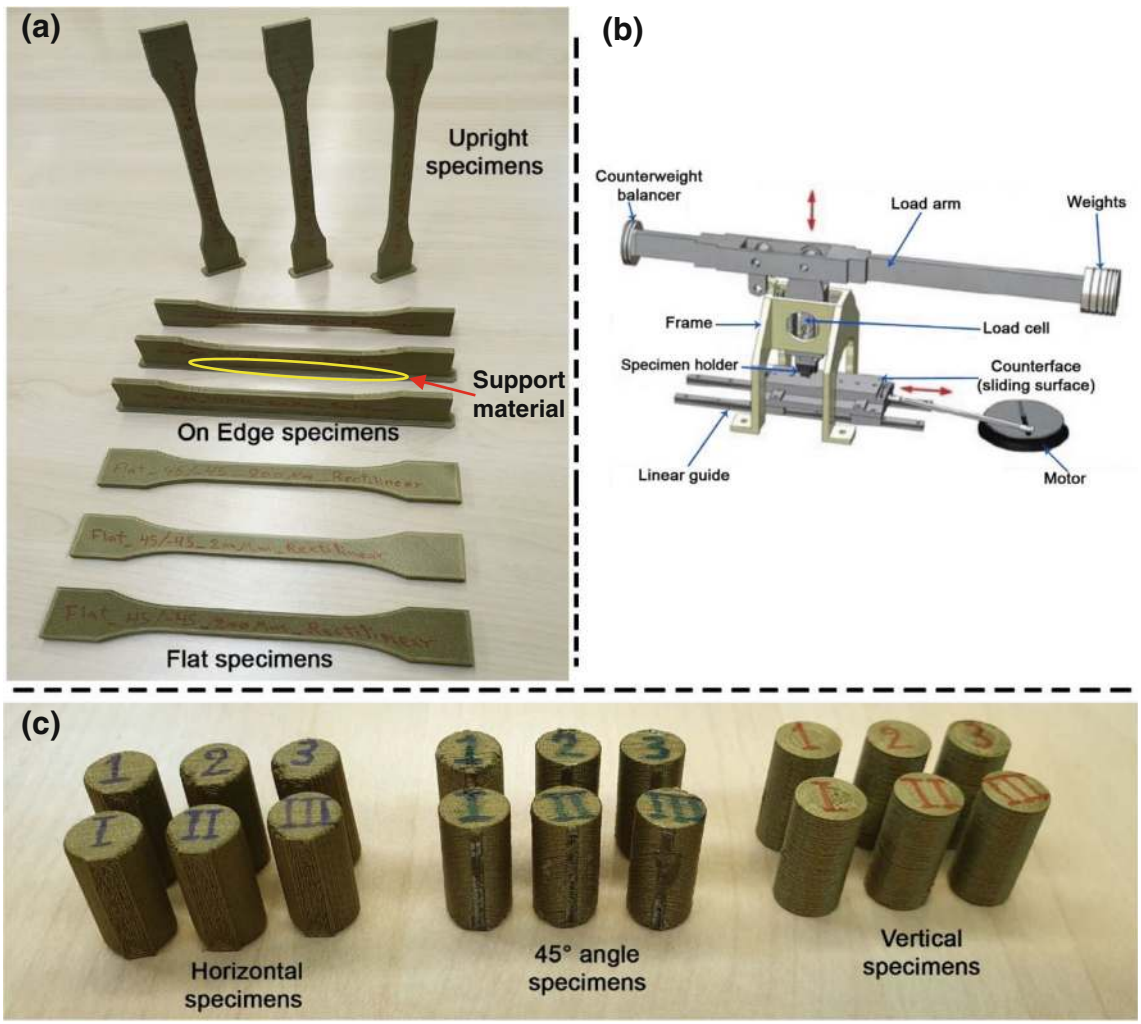

Fig. 2 **a**3D-printed tensile specimens before performing the test; **b** the schematic of cylinder-on-plate reciprocating tribometer apparatus [28]; **c** 3D-printed tribology test specimens

After adjusting the desired load, the weight can be fixed with a screw on the load arm.

The tribological measurements were performed at the tribotest laboratory in Szent István University under the laboratory conditions. The first step in the measurement process is to connect the measuring circuit, which consists of a computer, Spider 8 measuring converter, a tribometer, and an inverter. Spider 8 is a strain gauge measurement device for measuring the friction force and other essential features, various sensors in the measuring system are required. The test parameters which were employed during the tribology test are listed in Table 1.

The tribology test specimens which were 3D-printed with a height of 15.2 mm and a diameter of 8 mm are shown in Fig. 2c. All the test pieces were manufactured with a thickness of 0.2 mm. The specimens that distinguished with the Arabic numbers and Roman numerals were subjected to the applied load of 150 N and 200 N respectively. While blue, green, and red colors represent the print in Horizontal, 45° angle, and Vertical orientation consecutively.

2.5 Hardness, surface roughness, and optical microscope

The hardness test was carried out using a test device according to Shore D. This type is specified for testing thermoplastics, hard rubber, and hard plastics. A steel needle in the form of a point is pressed into the testing material, and the penetrating resistance amount is indicated at a scale. This method is standardized according to ASTM D2240 [40].

The surface roughness was acquired by employing a Mitutoyo testing instrument. Zoom in for the measurement sensor (probe) is displayed on the right side. Studying the surface profile helps to evaluate the quality of printing and to understand the tested sliding surfaces before and after tribology tests.

A computerized microscope ZEISS brand and a high quality digital camera with four magnification lenses (× 10, × 20, × 50, and × 100) were utilized to capture images. These images have been taken for the surface structure of 3D-printed specimens before and after tribology and tensile tests at different magnifications.

Table 1 Parameters of tribology test

Parameter	Value
Surface roughness of steel counterpart, R_a (μm)	0.08
Load, F (N)	150 and 200
Alternating motion frequency, f (Hz)	10
Stroke length, (mm)	6
Relative humidity, Rh (%)	50
Ambient temperature (°C)	23

3 Results and discussion

3.1 Determination of print accuracy

A digital Vernier caliper was used to measure the dimensions of the tensile and tribology test specimens. The accuracy average of the tensile test pieces is exhibited in Fig. 3. As mentioned in Section 2.2, the width and thickness dimensions were examined at three points within the gauge area for each specimen. The apparent results are given in comparison with the nominal value (width "b" = 10 mm and thickness "h" = 4 mm). No significant difference was observed among the dimensions of the tested samples. Nevertheless, in some cases, there was a slight reduction due to the effect of the number of layers. The FDM printing technique is related to anisotropic behavior and defect distribution. The internal structure between the bottom and top layer contains wider roads (print lines) and road-to-road defects compared to the road thickness of the bottom and top layers [41]. Hence, a greater number of layers increase the deformation because of the presence of these defects. The contour (shell) of each layer also influences the dimensions, as small contour size reduces shrinkage and improves accuracy, whereas large contour size can induce significant variation in temperature over the build platform. Internal stress arises as a result of cooling at different rates in different areas of the part and in turn causes print deformation and, implicitly, warping or shrinkage.

Theoretically, the best width results are expected to be in Flat-oriented samples. However, the test results show a significant similarity between Flat and Upright orientations, while the On-Edge test pieces reported the highest accuracy since its contour was smaller than the Flat. In the case of thickness, a large error bar can be noticed in the thickness of the Flat sample. This is due to the fact that the number of layers (thickness of specimen (4 mm)/layer thickness (0.2 mm) = number of layers (20)) required for manufacturing the thickness of this specimens is much more than the other orientation specimens (only one layer in both On-Edge and Upright). Thus, as a result of more layers, distorted growth becomes a dominant factor [42] resulting in poor dimensional accuracy. The best thickness accuracy is noticed in Upright specimens due to the much smaller contour than the Flat and On-Edge cases, which decreases the deformation. As for the accuracy average of all orientations, a percentage of 98.22% and 99.04% were obtained for thickness and width respectively in front of the nominal dimensions.

Concerning tribology specimens, the true values are a diameter (d) of 8 mm and length (L) of 15.2 mm. The length was measured at three different points. For diameter, the

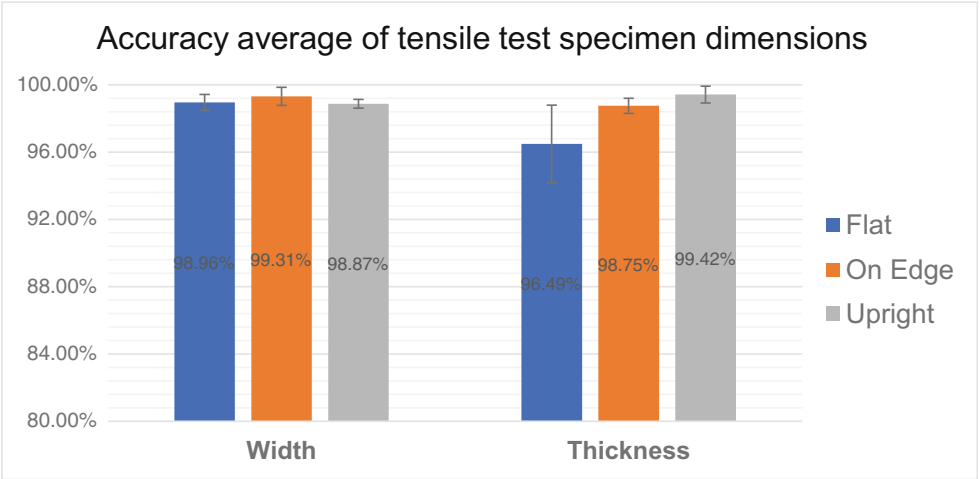

Fig. 3 Accuracy average for tensile test specimens printed in different orientations

measurements were taken at both cylinder edges on the *X* and *Y* axis. As illustrated in Fig. 4, the Vertical and Horizontal specimens acquired similar diameter accuracy. Nonetheless, 45° angle specimens reported the worst dimensional accuracy (which was expected) with the greatest standard deviation error bar. This is due to the positioning of the layers (tilted layers) and the influence of gravity during curing which increases the possibility of distortion. All specimens show high precision regarding the length which is in a good agreement with the nominal value. The print accuracy is resulting in an average of 98.19% for the diameter and 99.65% for the length in comparison with the basic size. Hence, the overall average for both tensile (thickness and width) and tribology (diameter and length) test specimens conducts a processing accuracy of 98.78%.

3.2 Tensile testing analysis

The tensile test results are revealed in Fig. 5. It can be clearly seen that curves are categorized into three groups in accordance with the tensile properties. Among the tested specimens, the Flat was the most ductile, whereas the On-Edge is the strongest; meanwhile, the Upright was the most brittle. The On-Edge specimens obviously could withstand almost double of the stress load that has been applied on the Flat and Upright ones.

For a better understanding of these groups' tendencies, the structure of the printed tensile test specimens is displayed in Fig. 6. Every layer contains the contour (shell) and the inner lines. In the case of Flat test pieces, the direction of the layers' contour is parallel with the applied force of the tensile test. As the long inner lines were built at a 45° angle with a moderate number of layers, that increases the possibility of these samples for more elongation (higher strain). The On-Edge workpiece has a complicated structure since its cross-section possesses a relatively small size contour with a massive number of layers and short inner lines. This interprets the high strength that these samples offered when pulled during the test. Concerning the Upright samples, the layers are built vertically up to

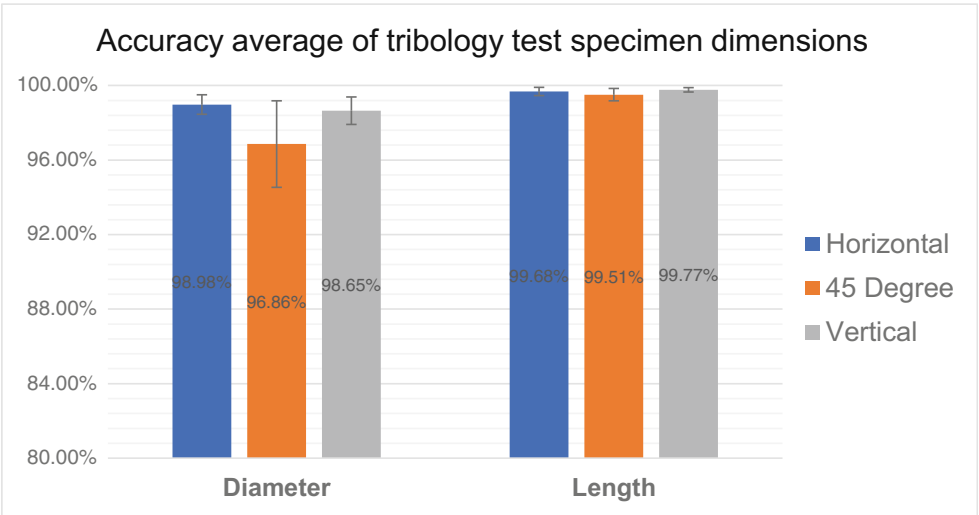

Fig. 4 Accuracy average for tribology test specimens printed in different orientations

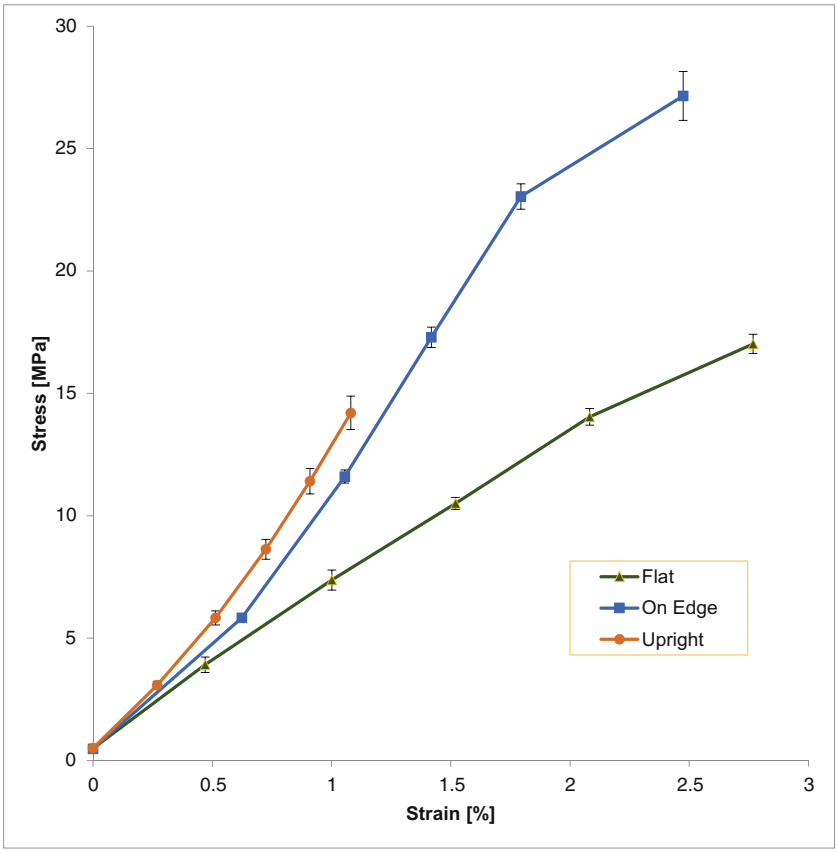

Fig. 5 Average of stress-strain curves for the specimens of different print orientation

each other and are not interlocked by the printed inner lines but only by the adhesion among layers. Therefore, these specimens are quickly fractured when stretched by the applied force, which makes its attitude brittle.

The provided results are in good agreement with the prior studies. Zaldivar et al. [43] examined the influence of print orientation on the mechanical behavior of ULTEM 9085 material. They stated that On-Edge samples obtained the highest

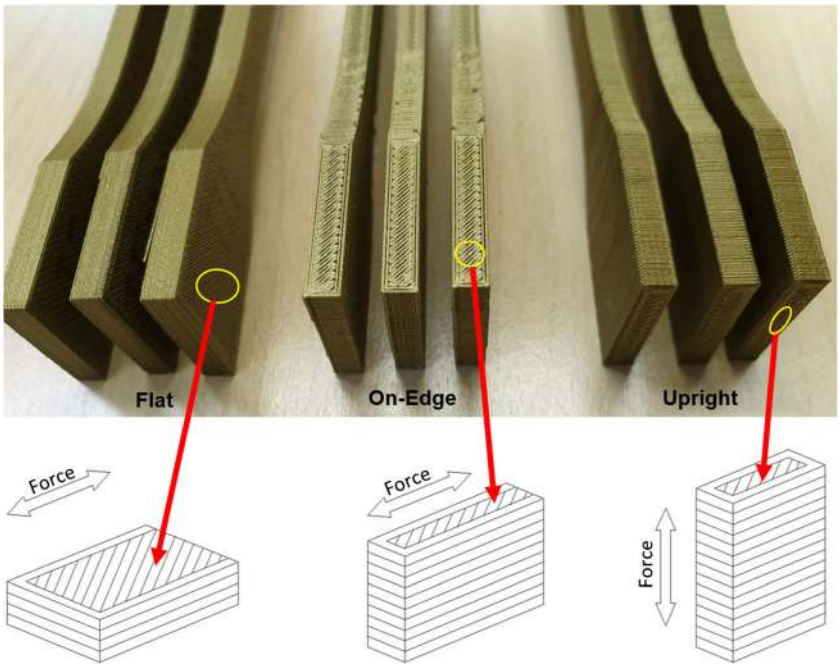

Fig. 6 Structure of 3D-printed tensile test specimens

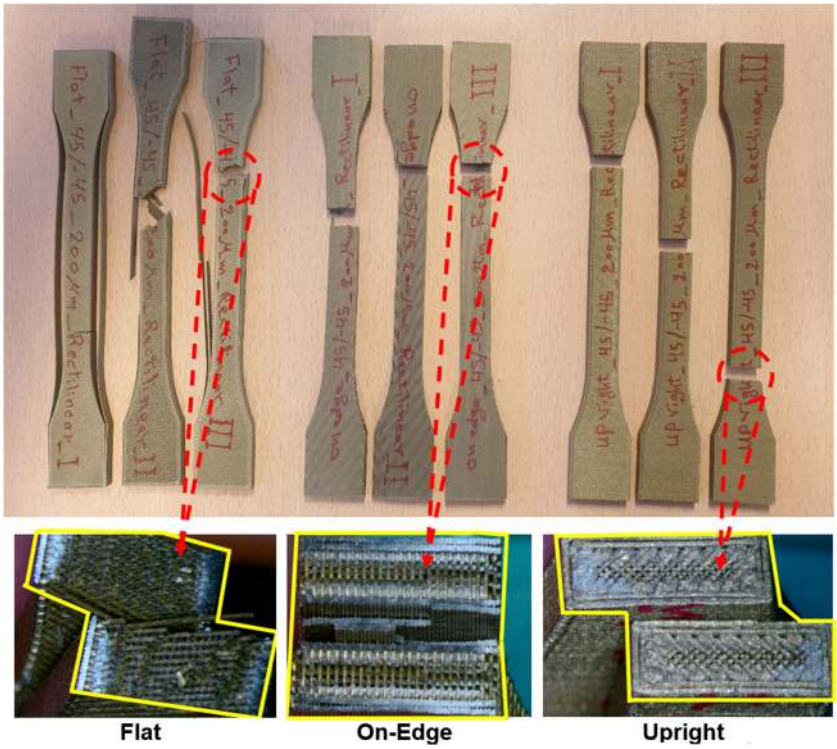

Fig. 7 The fracture form of specimens after the tensile test

measured tensile strengths with a difference of over 84% against the lowest tensile strengths which were observed in the Upright specimens, while the tensile strengths of Flat test pieces increased with an average of 21% than the Upright. These findings prove an almost similar trend in terms of the effect of print orientation as compared with the current work. The mechanical properties of polycarbonate parts FDM-printed were studied by Domingo-Espin et al. [44]. They explained the deformation behavior at break printed specimens in different orientations. Flat and On-Edge samples revealed a significant plastic behavior since the deposited filaments are organized in the same direction where the specimen is being pulled. Hence, contour and raster are longitudinally pulled. However, the fracture of the Upright specimen is fragile because no much plastic deformation was observed. This was due to the applied tension load during the test which was perpendicular to the built layers, where bonding strength in between is weaker than the resistance of pulled contours.

Thus, the orientation of layer formation is fundamental in terms of strength. The results clearly show that the tensile strength of the bonding between the layers is significantly less than the strength of the inner lines. This can also be explained further in Fig. 7, where the samples are shown after the fracture. The Flat specimen (left side) was broken with an angle of 45° which is similar to its raster direction angle structure. For all specimens of this print orientation, it can be noticed that the shell was dislocated after the tensile test. However, the robust construction of the inner lines, as well as the doubled shell layers, gave the On-Edge test piece (at the middle) a higher tensile strength. Obviously, the Upright sample (right side) was fractured in a sharp form. This was due to the fabric of the layers which was built vertically (up to each other) and perpendicular to the tension force. That led to separate the bonding between layers without any deformation in the shell or the inner lines.

3.3 Tribological properties analysis

The tribology measurements are obtained using Spider 8 (strain gauge measurement device) for measuring data of wear and friction force. CATMAN software program is employed to process the measured data which are transferred via Spider 8 through a computer. The experiment starts when the 3D-printed specimen slides against the counterpart of the tribometer. Wear and the friction force of the specimen are obtained as a function of total sliding distance. It is necessary to extract the static and dynamic friction coefficients per cycle, as demonstrated in Fig. 8a. The maximum values of measured points per half period were considered as the static coefficient of friction, while the average is the dynamic friction coefficient. The measured frictional force is negative in each half period because it was measured utilizing an alternating motion system. Therefore, the absolute value should be taken for the obtained negative frictional force.

The static and dynamic friction coefficient behavior for one of the specimens during the test is illustrated in Fig. 8b. At the beginning of measurement appears a slight difference between the static (blue) and dynamic (red) friction values. This can be explained as a measurement error due to the looseness in the

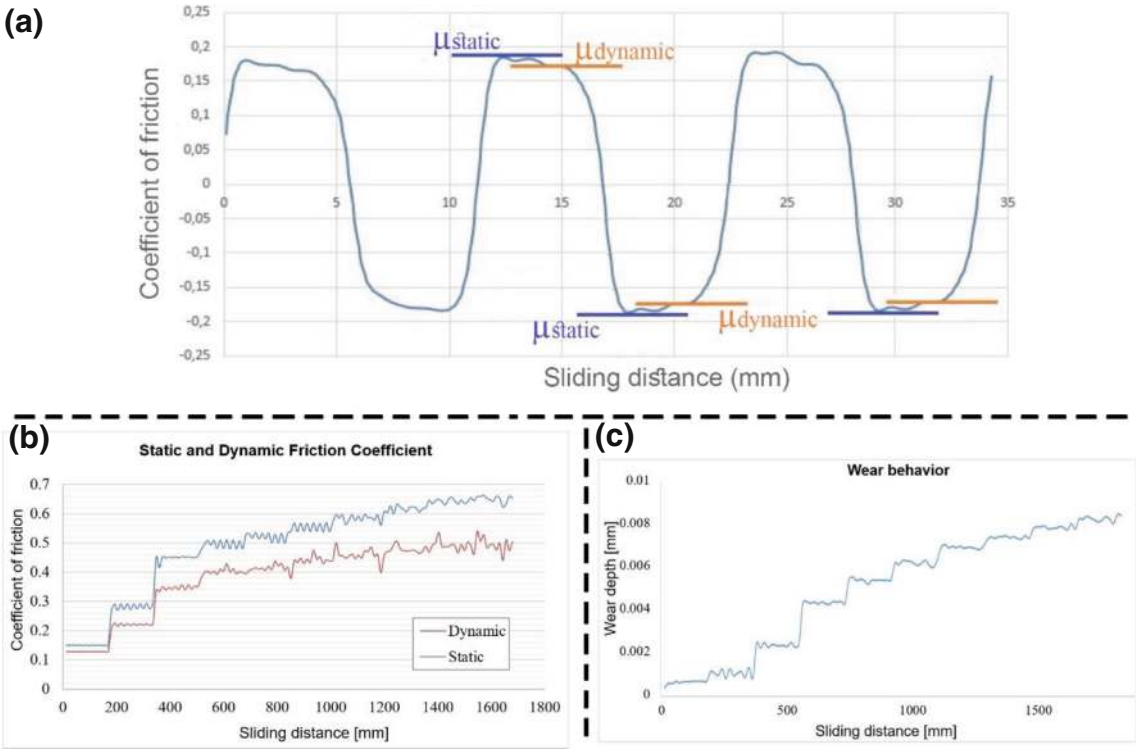

Fig. 8 **a** Static and dynamic friction coefficient per cycle; **b** static and dynamic friction coefficient curves; **c** wear behavior (a horizontally printed specimen, tribology test load 150 N)

sample clamp head of the tribometer. The difference between static and dynamic friction coefficient is increasing throughout the test time, which reveals that the stick-slip phenomenon is existent. The static friction is always higher than dynamic friction during the running time except for the starting moment. The wear behavior of one of the tested samples during the tribology test is demonstrated in Fig. 8c. Most of the samples have disclosed a persistent increment tendency in terms of wear rate versus the sliding distance.

After evaluating the tribology test results, the static and dynamic friction coefficient has been obtained. The main points of the investigated data are summarized in Fig. 9a. Considering both load (150 N and 200 N) results, it can be seen that Horizontal and 45° angle have the least dynamic friction coefficient. This makes them more appropriate for application purposes. However, the Vertical offered the highest friction coefficient values. That can be expounded due to the layers' structure, which is in contact with the sliding surface. However, it can be noticed a bigger difference between the dynamic and static friction coefficients under the load of 150 N. What it means is that sliding under lower loads increases the tendency for occurring stick-slip phenomenon, as it was possible to hear higher noise while testing Vertical specimens, which indicates the happening of this phenomenon as well. Bearing in mind that under the higher load (200 N), these differences decreased, therefore, the instability of the sliding also decreases.

The friction strongly depends on the sliding surface structure. It is apparent in Fig. 9b that various print orientations result in different surface roughness. The smoothest surface is given by horizontal and the roughest by vertical orientation. This basically determines the pressure between the two paired surfaces, which denotes the importance of the surface structure.

The comparison among the average wear depth that occurred during the tribology test is displayed in Fig. 10. The test pieces exhibited similar behavior in all orientations against each applied load (150 and 200 N). At the lower load, less wear was observed. The vertically oriented samples showed the least wear, due to the layer structure, since its contact area with the sliding counterpart is smaller than the other print orientation samples, whereas the 45° angle and Horizontal workpieces have offered elevated wear attitude. This is because a bigger surface area is in contact with the sliding plate. Certainly, the lower wear rate specimens are preferable for many implementations.

The above demonstrates the considerable effect of the layer structure for the sliding contact surfaces on both friction coefficient and wear. This finding suggests optimizing the print orientation to be more suitable for each case of usage. In order to choose whether the whole print orientation of the product must be changed or only at the required working surface.

The dynamic friction coefficient of all examined orientations for the used material (bronze/PLA) has ranged with an

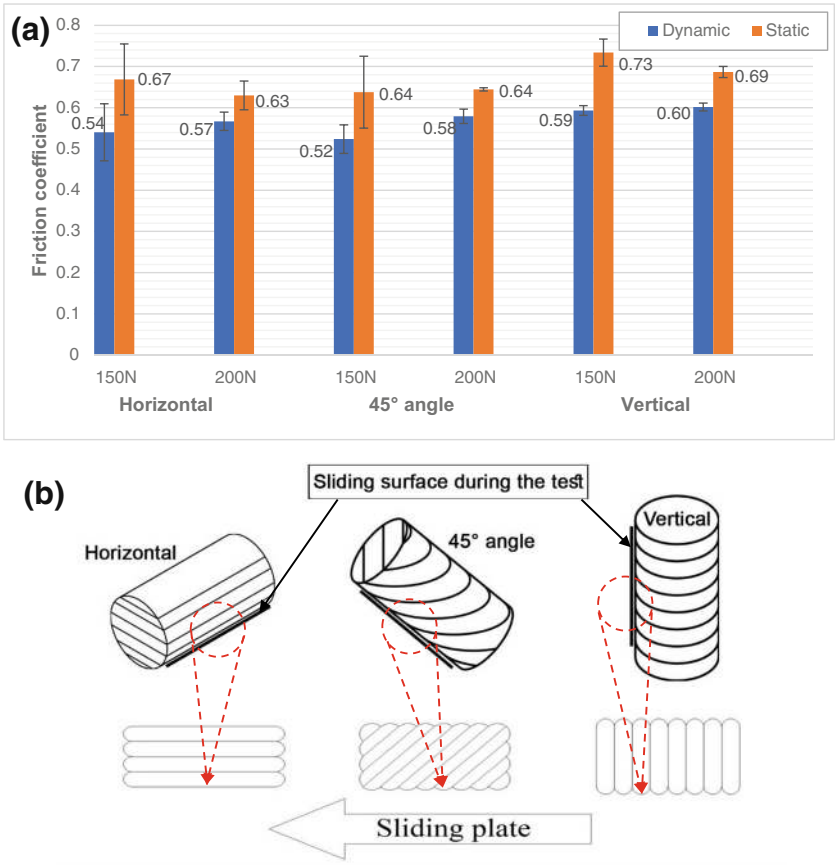

Fig. 9 **a** Comparison of average static–dynamic friction coefficient; **b** the contact surface structure

average of (0.52–0.6). The measured wear depth has averaged with values between (9.7 to 17.5 μm). These wear depth values give a specific wear rate about (3.3–6.1 $mm^3/N{\cdot}mm \times 10^{-9}$) respectively. Hence, in order to determine the influence of bronze existence on the tribological properties, the findings should be compared with wear and friction of neat PLA achieved in literature. Hanon et al. [45] reviewed the tribological behavior of 3D-printed PLA with two different colors. In general, the coefficient of friction for PLA has ranged with a value of approximately (0.5), while the wear depth of the white PLA was measured about (150 μm). The specific wear rate for neat PLA was calculated by Bajpai et al. [7]. When employing a relatively low load (30 N), the specific wear rate reached 3.2×10^{-9} $mm^3/N{\cdot}mm$. Comparing the present results with the prior studies indicates that bronze addition has improved the wear behavior of PLA, but kept the friction coefficient at the same range. This trend corresponds with what was mentioned by Unlu et al. [32] and Unal et al. [34], where the reinforcement by bronze has improved the wear resistance even if the friction more or less remains the same. Guo et al. [46] evaluated the influence of post-processing on tribology performance and surface

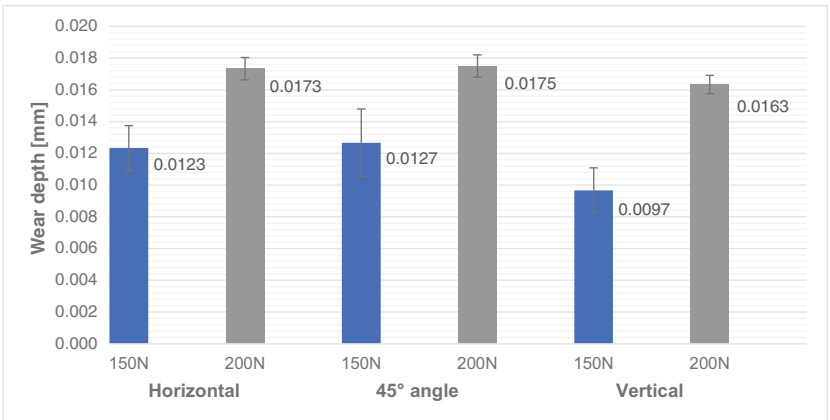

Fig. 10 Comparison of average wear depth for each print orientation

characteristics of polyamide 12 (PA12) specimens manufactured by selective laser sintering. The authors proposed subjecting the surfaces to the so-called magnetic field-assisted finishing (MFAF) as a post-processing method that comes after precision grinding. The processed surfaces presented a better tribology performance demonstrated by higher wear resistance and a lower coefficient of friction. This indicates the possibility of employing such post-processing methods to improve the tribological properties of 3D-printed polymers.

3.4 Determination of hardness and surface roughness

The hardness of three FDM manufactured specimens (one from each print orientation) was estimated using Shore D hardness measurements. The test was done on three points (gripping, curvature, and gauge sections) for each sample. The hardness ranges (63–67), (70–72), and (72.5–76) Shore D for Flat, On-Edge, and Upright print orientation specimens, respectively, as shown in Fig. 11. The highest values were reported at the Upright and On-Edge samples because the test penetration needle was in contact with the shell of the print, which is harder, while the needle was in contact with the filling face in the Flat test piece. The hardness of the bronze/polymer composite also depends on the incorporated volume percent of polymer particles [47]. Increasing polymer content reduces the hardness of the manufactured product. The soft nature of the polymeric particles is the main reason behind this trend. In terms of tribology, the effect of high hardness is that the roughness peaks are more rigid. Thus, when the contact zone in sliding, the harder material is more difficult to fit with the counterpart surface. This leads to smaller sliding surfaces that retain load (due to the lack of elastic deformation) result in higher surface pressures. These rigid asperities, as well as high surface pressure, encourage creating grooves in which boost the existence of abrasive wear. In contrast, the material with lower hardness (more elasticity) fits better with the counterpart surface which provides a larger sliding area. Hence, there will be less surface pressure and consequently fewer abrasion effects.

Surface roughness is very important for tribological behavior; it shows the condition of the sliding surface. The smoother surface gives a larger contact area during the sliding. Therefore, the adhesion will be increased, but meanwhile, the load will be decreased due to lower contact pressure.

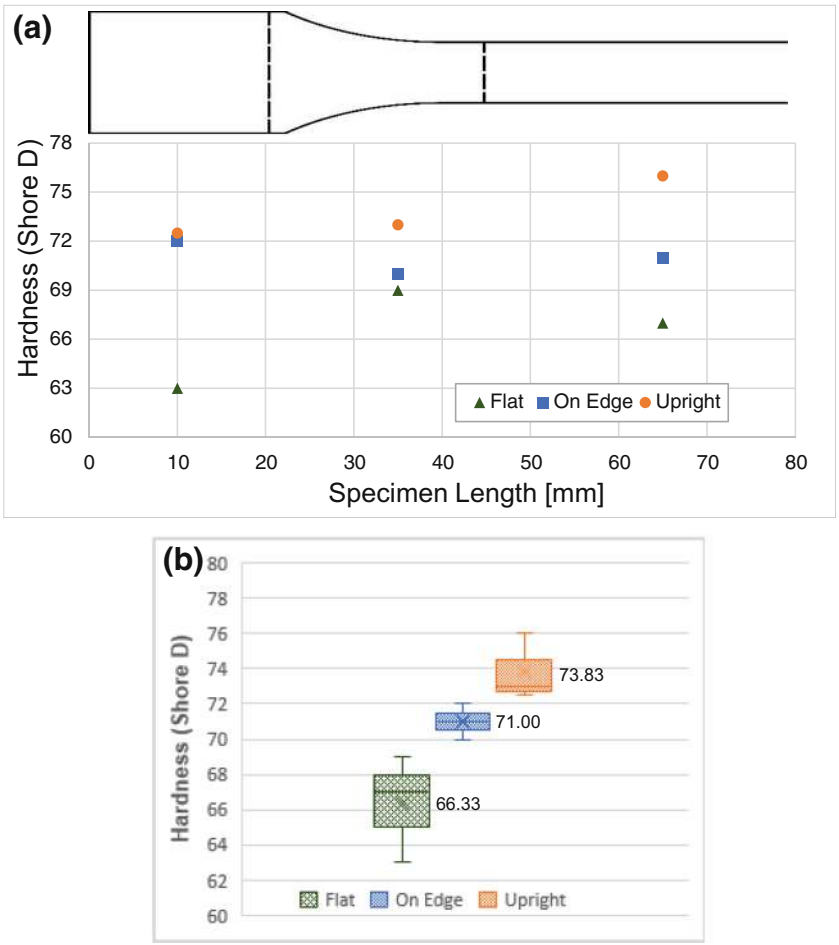

Fig. 11 **a** Hardness test results; **b** average of hardness results for different print orientations

Table 2 Surface roughness test results

Print orientation	Flat			On-Edge			Upright		
Point	1	2	3	1	2	3	1	2	3
R_a (μm)	14.29	15.84	15.03	12.32	12.46	12.64	16.69	17.25	16.89

The results of the surface roughness for the three examined orientations are presented in Table 2. The measured profile of each print orientation is shown in Fig. 12. The dark line at the right side of the figure illustrates the path of the measurement and the surface face where the test was done. In all cases, the measurement track was perpendicular to the layers build direction where the shell can be found. The surface roughness (R_a) values were verified based on the average of R_a results for each print orientation at the layer thickness of 200 μm. It can be clearly seen that a slight difference has been observed among the tested surfaces which ranged between 12.6 and 16.8 μm. The smoothest surface was noticed at the On-Edge sample. This is due to peaks and valleys of the entire layers which seem quite uniform and its depth is insignificant. Nevertheless, the Upright specimen reflected the roughest surface since the structure contains non-regulated layers due to the stacking of the printed material. Lee et al. [48] have demonstrated a similar range of roughness (12.6 μm) for a microfluidic channel wall FDM-printed at a 90° inclined angle (alike the present shell). They mentioned that surfaces generated through FDM printers are rather rough, where the profile of roughness is distinguished by a stepping feature. As for the

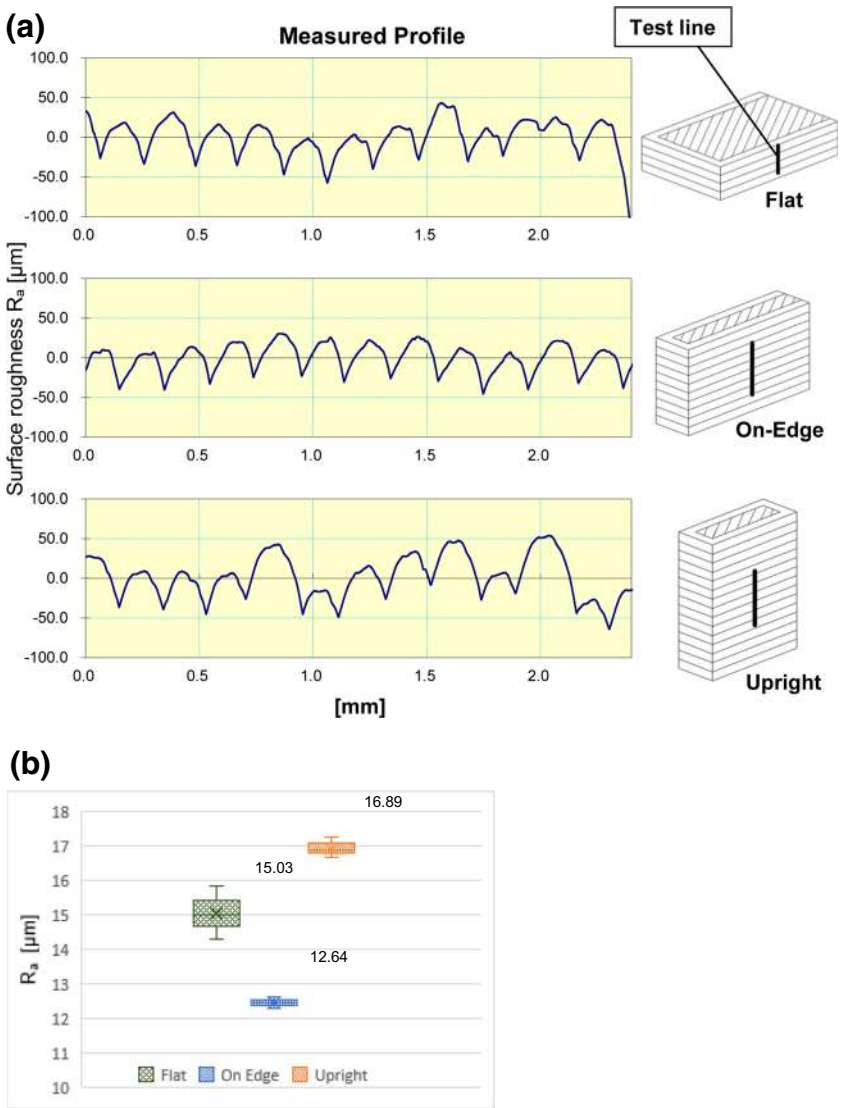

Fig. 12 **a** Surface roughness measured profile comparison; **b** surface roughness, R_a average comparison

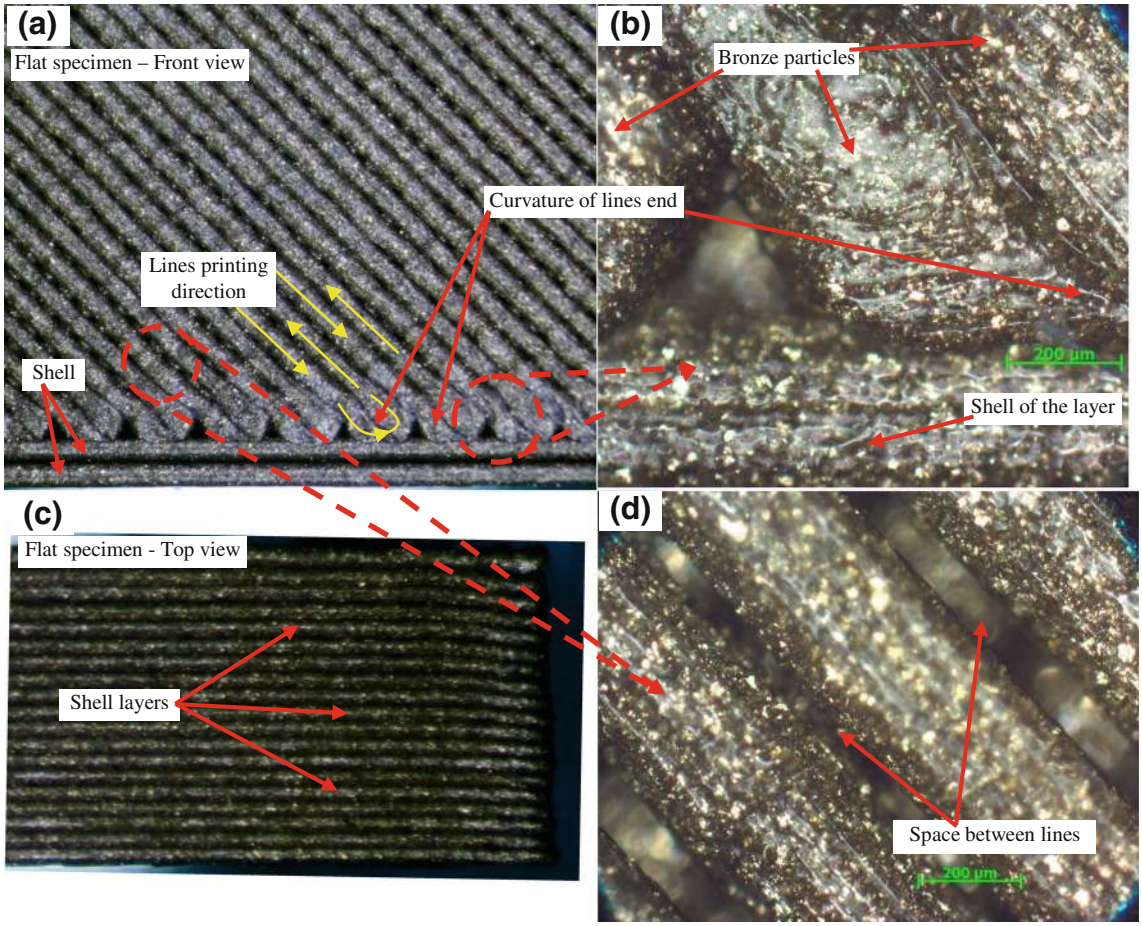

Fig. 13 Surface structure images of the 3D-printed sample in Flat orientation

bronze particles influence, Balaji et al. [47] inspected the surface roughness of mild steel substrate coated by bronze/PTFE composite. They concluded that R_a values vary in accordance with the content of the bronze and polymer deposit. The higher the bronze content is, the smoother the surface roughness, and vice versa. The effect of the surface roughness on tribological properties lies as the smoother the surface the bigger the sliding contact area that leads to less pressure but higher wear. While the more roughness due to the asperities results in a higher pressure, thus a higher friction coefficient there is. Finally, the obtained values of surface roughness (R_a) in this research can be improved by means of post-processing procedures like surface polishing.

3.5 Surface structure analysis

Micrographs of the surface morphology are shown in Figs. 13, 14, 15, and 16. The surface structure images of Flat orientation 3D-printed bronze/PLA specimen from the front and top view are offered in Fig. 13a–d. The random distribution of the bronze particles is clearly observed in the specimens. The layers were printed with a raster direction angle of 45°/135° (i.e., one layer with 45° while the upper one is 135° and so on). This direction angle as well as the curvature at the end of every built line has been illustrated. Despite the print infill setting is 100%, spaces among lines have been observed in the specimens, which indicates the anisotropy of the FDM method. These lines in every layer are surrounded by a double strap of the shell (contour). The shell texture from the front and top view are also exhibited.

The microscopic examination of the On-Edge orientation specimen is shown in Fig. 14a–d. Short printing lines have been observed at the top view (seen in Fig. 14c). These short lines are supported by the interlocked layers (which were built layer by layer) as well as the assist of the shell. The samples of this orientation possess a substantial amount of shell compared with the length of the lines in every layer. These factors (short lines, the interlocking of layers, and the shell amount feature) grant the On-Edge specimen strength more than other orientation specimens. This interprets why the On-Edge specimens could afford twice the applied tensile load in comparison with the others. The angle between lines of layers was confirmed as 90° (manifested in Fig. 14d) since the angle of the raster direction for the first layer is 45°, while the second is 135°.

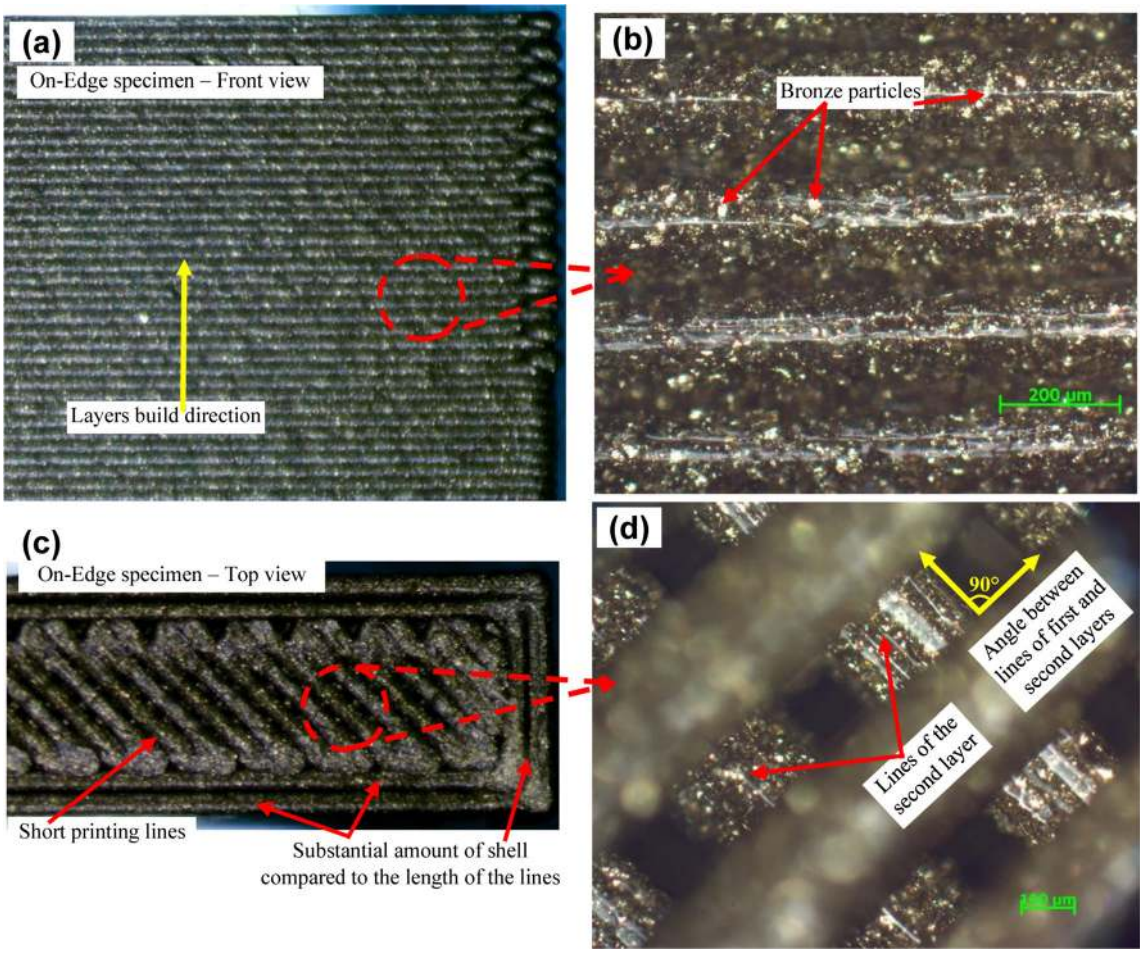

Fig. 14 Microscopic examination of On-Edge orientation specimen

The front and top views of the Upright specimen have been demonstrated in Fig. 15a–d. A unique construction like the strands has been observed at the edges (binds the shell layers) of this sample (presented in Fig. 15c, d). The Upright sample has been characterized by a weak tensile strength. This was due to the layers of the test piece which were built perpendicularly to the applied force of the tensile test. The adhesion bonding is the only linkage since there are no merged lines or fibers among the layers.

Micrographs of the perimeter morphology of bronze/PLA cylindrical specimens before and after the tribology test are shown in Fig. 16a–d. The surface structure after the tribology test for the Horizontal, 45° angle, and Vertical print orientation samples has been exhibited in Fig. 16b–d, respectively. The essential points associated with the surface morphology of the worn area were demonstrated. At the Horizontal print orientation sample, the worn area is pigmented with black color (displayed in Fig. 16b). This is because of the large contact area with the counterpart, which results in a higher wear rate for test pieces. It can be observed that after sliding at different conditions, most of the bronze particles are still in its locations. These particles are in good condition, and no pull out or detachment was noticed. The existence of an abrasive wear mechanism was confirmed by the microscope images of different print orientations, which showed marks of pitting and grooves (as disclosed in Fig. 16c, d). Those asperities contributed to alteration of the surface roughness, which influenced the tribological behavior. In the obtained tribology results, the decreased wear loss of the vertically orientated sample, despite the higher coefficient of friction, was due to the higher roughness of the surface. This confirmed the high pressure prevailing between the sliding surfaces due to the lower contact area. In contrast, the horizontally orientated test piece revealed a relatively lower surface roughness that caused a higher wear depth but a lower friction coefficient. The extent of sliding distance also affects the surface roughness and, implicitly, the wear behavior. When wear occurs, the surface of the specimen has a higher roughness. Hence, the top layer wears off easily, presenting a higher wear rate. As the sliding distance increase, the high slope of the wear rate decreases. As wear progresses, a glaze forms on the specimen sliding surface, which cause a significant reduction in the rate of wear.

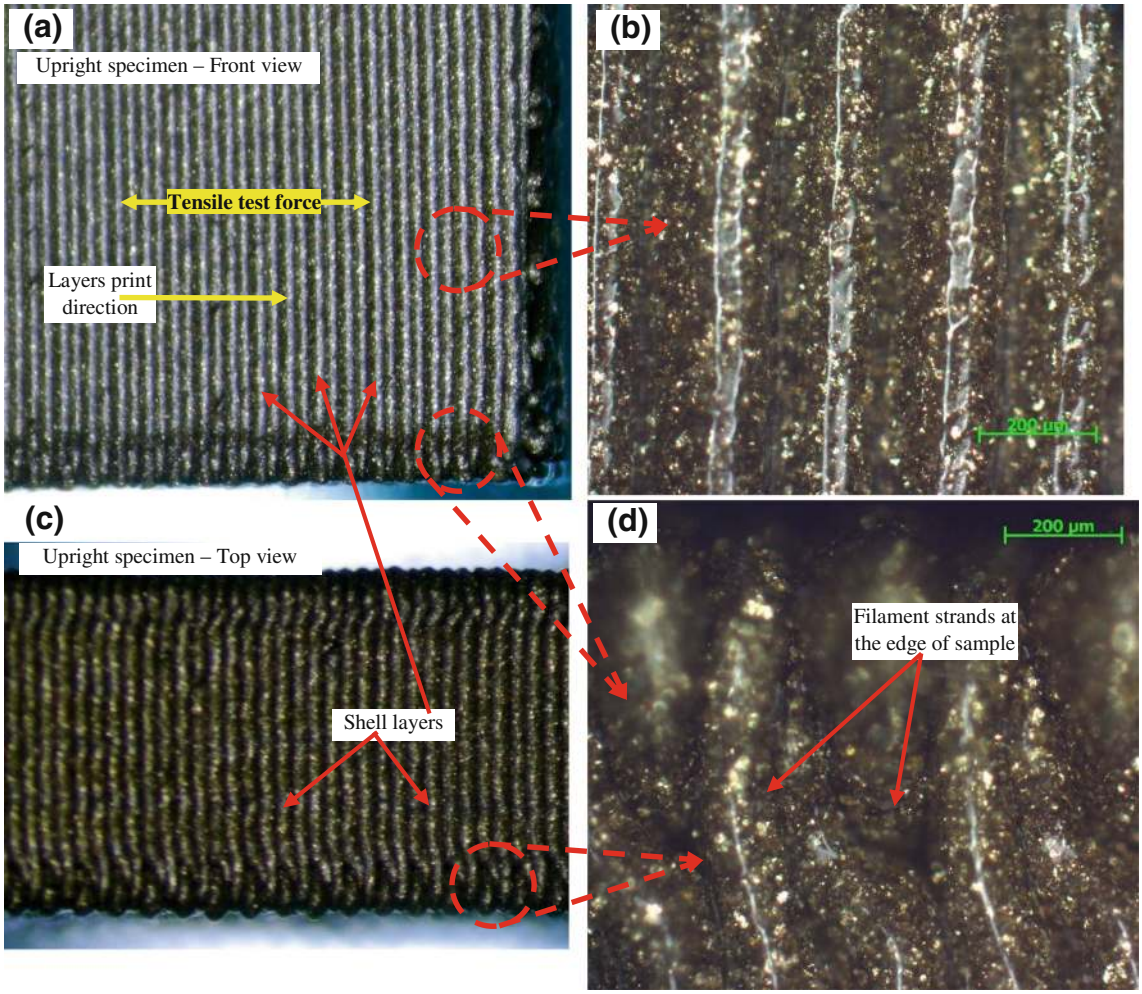

Fig. 15 The surface structure of the Upright specimen from the front and top view

4 Conclusions

In the present study, the tribological and mechanical properties of 3D-printed bronze/PLA composite material have been evaluated. According to the results obtained, the following conclusions can be drawn:

- The commercial FDM 3D printers could be utilized as an affordable and good quality alternative for fabricating functional parts with high accuracy of 98.78% against its nominal dimensions.
- The FDM printing parameters, particularly the print orientation, significantly influence the mechanical and tribological behavior of 3D-printed products.
- The On-Edge print orientation revealed maximum tensile stress of 28 MPa, which was almost twice the stress value as compared with Flat and Upright specimens. The Upright sample showed a very fragile behavior, with extremely rapid fracturing of the printed layers with 1.1% elongation at the break point. Meanwhile, the Flat and On-Edge samples exhibited a more plastic behavior, with an elongation of 2.5–3% at the break point.
- Regarding the tribological tests that were performed under a dry condition and reciprocating sliding movement, the structure of the sliding surfaces played a key role in determining wear and friction. The smaller the contact area (rough surface) between the sliding surfaces is, the higher the coefficient of friction (due to the high pressure) but the lower the wear rate was, and vice versa. The vertically oriented test pieces showed the highest friction but the least wear.
- The occurrence of the stick-slip phenomenon was more likely in the context of sliding under low loads, but wear was diminished.
- The presence of bronze particles as a reinforcement for the PLA material improved the tribological properties since the wear depth was significantly decreased as compared with the literature. Nevertheless, the friction remained more or less the same, since the matrix of the polymer composite was filled with hard particles.

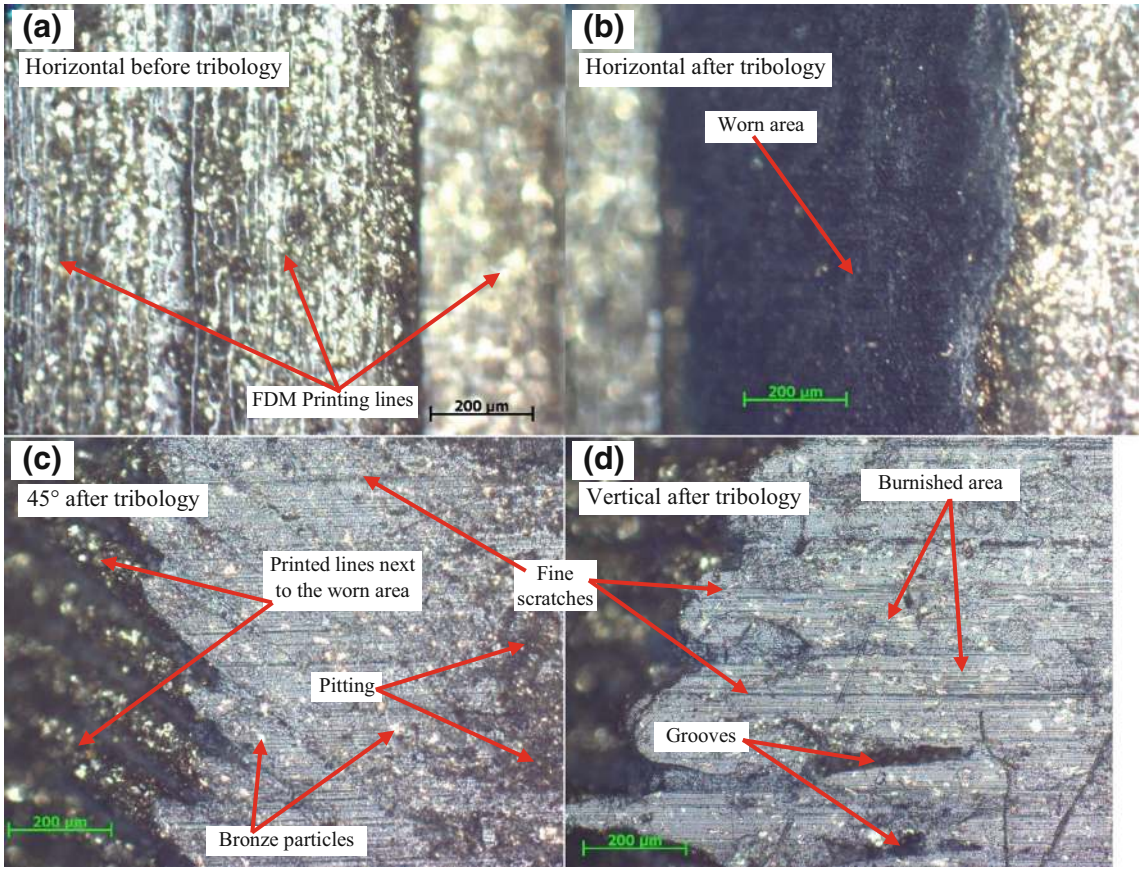

Fig. 16 Surface morphology of FDM specimens printed in Horizontal, 45° angle, and vertical orientation before and after tribology test

– The Upright and On-Edge samples disclosed a higher hardness (73.8 and 71 Shore D), which could be attributed to the fact that the test needle was in contact with the shell of the print, which was more solid. Meanwhile, the Flat samples displayed lower hardness (66.3 Shore D), due to the contact with the inner print filling which was less solid than the shell.

To summarize, the results demonstrate that bronze subsistence and print orientation, and implicitly, the layer structure of the sliding contact surfaces, have a considerable effect on both the friction coefficient and wear as well as on other mechanical properties. This finding suggests that the print orientation settings should be optimized during product manufacture to suit a certain application.

Future work could explore the influence of additional parameters related to 3D printing settings (e.g., layer thickness, other print orientations, infill percentage and pattern, and raster direction angle) on the tribological properties. As for the material content, it is suggested that bronze reinforcement should be bolstered, as this can lead to remarkable enhancements that are reflected in the wear and friction behavior. Therefore, 3D-printed parts can be confirmed to be potential candidates for industrial sliding applications, such as bearings and bushings at low speed.

Funding information Open access funding provided by Szent István University (SZIE). This work was supported by the Stipendium Hungaricum Programme and by the Mechanical Engineering Doctoral School, Szent István University, Gödöllő, Hungary.

References

1. Vaezi M, Seitz H, Yang S (2013) A review on 3D micro-additive manufacturing technologies. Int J Adv Manuf Technol 67:1721–1754. https://doi.org/10.1007/s00170-012-4605-2
2. Dizon JRC, Espera AH, Chen Q, Advincula RC (2018) Mechanical characterization of 3D-printed polymers. Addit Manuf 20:44–67. https://doi.org/10.1016/j.addma.2017.12.002
3. Liu Z, Wang Y, Wu B, Cui C, Guo Y, Yan C (2019) A critical review of fused deposition modeling 3D printing technology in

manufacturing polylactic acid parts. Int J Adv Manuf Technol 102: 2877–2889. https://doi.org/10.1007/s00170-019-03332-x
4. Wu W, Geng P, Li G, Zhao D, Zhang H, Zhao J (2015) Influence of layer thickness and raster angle on the mechanical properties of 3D-printed PEEK and a comparative mechanical study between PEEK and ABS. Materials (Basel) 8:5834–5846. https://doi.org/10.3390/ma8095271
5. Cantrell JT, Rohde S, Damiani D, Gurnani R, DiSandro L, Anton J, Young A, Jerez A, Steinbach D, Kroese C, Ifju PG (2017) Experimental characterization of the mechanical properties of 3D-printed ABS and polycarbonate parts. Rapid Prototyp J 23:811–824. https://doi.org/10.1108/RPJ-03-2016-0042
6. Serra T, Planell JA, Navarro M (2013) High-resolution PLA-based composite scaffolds via 3-D printing technology. Acta Biomater 9: 5521–5530. https://doi.org/10.1016/j.actbio.2012.10.041
7. Bajpai PK, Singh I, Madaan J (2013) Tribological behavior of natural fiber reinforced PLA composites. Wear 297:829–840. https://doi.org/10.1016/j.wear.2012.10.019
8. Li N, Li Y, Liu S (2016) Rapid prototyping of continuous carbon fiber reinforced polylactic acid composites by 3D printing. J Mater Process Technol 238:218–225. https://doi.org/10.1016/j.jmatprotec.2016.07.025
9. Tian X, Liu T, Yang C, Wang Q, Li D (2016) Interface and performance of 3D printed continuous carbon fiber reinforced PLA composites. Compos A Appl Sci Manuf 88:198–205. https://doi.org/10.1016/j.compositesa.2016.05.032
10. Blok LG, Longana ML, Yu H, Woods BKS (2018) An investigation into 3D printing of fibre reinforced thermoplastic composites. Addit Manuf 22:176–186. https://doi.org/10.1016/j.addma.2018.04.039
11. Akhoundi B, Behravesh AH, Bagheri Saed A (2019) An innovative design approach in three-dimensional printing of continuous fiber–reinforced thermoplastic composites via fused deposition modeling process: in-melt simultaneous impregnation. Proc Inst Mech Eng B J Eng Manuf 234:243–259. https://doi.org/10.1177/0954405419843780
12. Kariz M, Sernek M, Obućina M, Kuzman MK (2018) Effect of wood content in FDM filament on properties of 3D printed parts. Mater Today Commun 14:135–140. https://doi.org/10.1016/j.mtcomm.2017.12.016
13. Lee JT, Kim MW, Song YS, Kang TJ, Youn JR (2010) Mechanical properties of denim fabric reinforced poly(lactic acid). Fibers Polym 11:60–66. https://doi.org/10.1007/s12221-010-0060-6
14. Murphy CA, Collins MN (2018) Microcrystalline cellulose reinforced polylactic acid biocomposite filaments for 3D printing. Polym Compos 39:1311–1320. https://doi.org/10.1002/pc.24069
15. Hanon MM, Marczis R, Zsidai L (2019) Anisotropy evaluation of different raster directions, spatial orientations, and fill percentage of 3D printed PETG tensile test specimens. Key Eng Mater 821:167–173. https://doi.org/10.4028/www.scientific.net/KEM.821.167
16. Ziemian CW, Cipoletti DE, Ziemian MN, Haile KV (2014) Monotonic and cyclic tensile properties of ABS components fabricated by additive manufacturing. Proc 25th Int Solid Free Fabr Symp 525–541. https://doi.org/10.2138/am.2007.2540
17. Rybachuk M, Alice Mauger C, Fiedler T, Öchsner A (2017) Anisotropic mechanical properties of fused deposition modeled parts fabricated by using acrylonitrile butadiene styrene polymer. J Polym Eng 37:37–706. https://doi.org/10.1515/polyeng-2016-0263
18. Vega V, Clements J, Lam T, Abad A, Fritz B, Ula N, Es-Said OS (2011) The effect of layer orientation on the mechanical properties and microstructure of a polymer. J Mater Eng Perform 20:978–988. https://doi.org/10.1007/s11665-010-9740-z
19. Sood AK, Ohdar RK, Mahapatra SS (2010) Parametric appraisal of mechanical property of fused deposition modelling processed parts. Mater Des 31:287–295. https://doi.org/10.1016/j.matdes.2009.06.016
20. Weng Z, Wang J, Senthil T, Wu L (2016) Mechanical and thermal properties of ABS/montmorillonite nanocomposites for fused deposition modeling 3D printing. Mater Des 102:276–283. https://doi.org/10.1016/j.matdes.2016.04.045
21. Türk D-A, Brenni F, Zogg M, Meboldt M (2017) Mechanical characterization of 3D printed polymers for fiber reinforced polymers processing. Mater Des 118:256–265. https://doi.org/10.1016/j.matdes.2017.01.050
22. Croccolo D, De Agostinis M, Olmi G (2013) Experimental characterization and analytical modelling of the mechanical behaviour of fused deposition processed parts made of ABS-M30. Comput Mater Sci 79:506–518. https://doi.org/10.1016/j.commatsci.2013.06.041
23. Quan Z, Suhr J, Yu J, Qin X, Cotton C, Mirotznik M, Chou TW (2018) Printing direction dependence of mechanical behavior of additively manufactured 3D preforms and composites. Compos Struct 184:917–923. https://doi.org/10.1016/j.compstruct.2017.10.055
24. Sood AK, Ohdar RK, Mahapatra SS (2012) Experimental investigation and empirical modelling of FDM process for compressive strength improvement. J Adv Res 3:81–90. https://doi.org/10.1016/j.jare.2011.05.001
25. Ayrilmis N, Kariz M, Kwon JH, Kitek Kuzman M (2019) Effect of printing layer thickness on water absorption and mechanical properties of 3D-printed wood/PLA composite materials. Int J Adv Manuf Technol 102:2195–2200. https://doi.org/10.1007/s00170-019-03299-9
26. Briscoe BJ, Sinha SK (2013) Tribological applications of polymers and their composites – past, present and future prospects
27. Hong Y, Zhang P, Lee K-H, Lee C-H (2017) Friction and wear of textured surfaces produced by 3D printing. Sci China Technol Sci 60:1400–1406. https://doi.org/10.1007/s11431-016-9066-0
28. Hanon MM, Marczis R, Zsidai L (2020) Impact of 3D-printing structure on the tribological properties of polymers. Ind Lubr Tribol. https://doi.org/10.1108/ILT-05-2019-0189
29. Bustillos J, Montero D, Nautiyal P, Loganathan A, Boesl B, Agarwal A (2017) Integration of graphene in poly(lactic) acid by 3D printing to develop creep and wear-resistant hierarchical nanocomposites. Polym Compos 16:101–113. https://doi.org/10.1002/pc.24422
30. Ertane EG, Dorner-Reisel A, Baran O, Welzel T, Matner V, Svoboda S (2018) Processing and wear behaviour of 3D printed PLA reinforced with biogenic carbon. Adv Tribol 2018:1–11. https://doi.org/10.1155/2018/1763182
31. Bai J, Yuan S, Chow W, Chua CK, Zhou K, Wei J (2015) Effect of surface orientation on the tribological properties of laser sintered polyamide 12. Polym Test 48:111–114. https://doi.org/10.1016/j.polymertesting.2015.09.017
32. Ünlü BS, Uzkut M, Atik E (2010) Tribological behaviors of polymer-based particle-reinforced PTFE composite bearings. J Reinf Plast Compos 29:1353–1358. https://doi.org/10.1177/0731684409103952
33. Conte M, Igartua A (2012) Study of PTFE composites tribological behavior. Wear 296:568–574. https://doi.org/10.1016/j.wear.2012.08.015
34. Unal H, Kurtulus E, Mimaroglu A, Aydin M (2010) Tribological performance of PTFE bronze filled composites under wide range of application conditions. J Reinf Plast Compos 29:2184–2191. https://doi.org/10.1177/0731684409345617
35. eSUN (2018) Safety data sheet of PLA bronze filament. Shenzhen, China, retrieved from: http://www.esunchina.net/UploadFiles/Download/MSDS_eSUN_PLA Bronze filament.pdf [Accessed: 29/12/2019]

36. International Organization for Standardization (2012) ISO 527-2: 2012: Plastics - Determination of tensile properties - Part 2: test conditions for moulding and extrusion plastics
37. International Organization for Standardization (2012) ISO 527-1: 2012 - Plastics – Determination of tensile properties – Part 1: General principles
38. Müller CMO, Laurindo JB, Yamashita F (2009) Effect of cellulose fibers on the crystallinity and mechanical properties of starch-based films at different relative humidity values. Carbohydr Polym 77: 293–299. https://doi.org/10.1016/j.carbpol.2008.12.030
39. Zsidai L, Kalácska G (2014) " Stick-slip" PA és PEEK kompozitok súrlódásánál henger/sík modell vizsgálati rendszerben Műanyag és Gumi 51:462–470
40. ASTM International (2015) ASTM D2240-15e1, Standard test method for rubber property—Durometer Hardness
41. Keleş Ö, Blevins CW, Bowman KJ (2017) Effect of build orientation on the mechanical reliability of 3D printed ABS. Rapid Prototyp J 23:320–328. https://doi.org/10.1108/RPJ-09-2015-0122
42. Mohamed OA, Masood SH, Bhowmik JL, Nikzad M, Azadmanjiri J (2016) Effect of process parameters on dynamic mechanical performance of FDM PC/ABS printed parts through design of experiment. J Mater Eng Perform 25:2922–2935. https://doi.org/10.1007/s11665-016-2157-6
43. Zaldivar RJ, Witkin DB, McLouth T, Patel DN, Schmitt K, Nokes JP (2017) Influence of processing and orientation print effects on the mechanical and thermal behavior of 3D-printed ULTEM® 9085 Material. Addit Manuf 13:71–80. https://doi.org/10.1016/j.addma.2016.11.007
44. Domingo-Espin M, Puigoriol-Forcada JM, Garcia-Granada AA, Llumà J, Borros S, Reyes G (2015) Mechanical property characterization and simulation of fused deposition modeling Polycarbonate parts. Mater Des 83:670–677. https://doi.org/10.1016/j.matdes.2015.06.074
45. Hanon MM, Kovács M, Zsidai L (2019) Tribology behaviour investigation of 3D printed polymers. Int Rev Appl Sci Eng 10:173–181. https://doi.org/10.1556/1848.2019.0021
46. Guo J, Bai J, Liu K, Wei J (2018) Surface quality improvement of selective laser sintered polyamide 12 by precision grinding and magnetic field-assisted finishing. Mater Des 138:39–45. https://doi.org/10.1016/j.matdes.2017.10.048
47. Balaji R, Pushpavanam M, Kumar KY, Subramanian K (2006) Electrodeposition of bronze–PTFE composite coatings and study on their tribological characteristics. Surf Coat Technol 201:3205–3211. https://doi.org/10.1016/j.surfcoat.2006.06.039
48. Lee JM, Zhang M, Yeong WY (2016) Characterization and evaluation of 3D printed microfluidic chip for cell processing. Microfluid Nanofluid 20:5. https://doi.org/10.1007/s10404-015-1688-8